

Article

Effect of Molybdenum Content on Microstructure and Mechanical Properties of Ti-Mo-Fe Alloys by Powder Metallurgy

Hyo-Woon Hwang ¹, Ji-Hwan Park ² and Dong-Geun Lee ^{1,*}

¹ Department of Materials Science and Metallurgical Engineering, Suncheon National University, Suncheon 57922, Korea; hyowoon7501@naver.com

² Material Technical Innovation Group (MTIG), Hwaseong-si 18574, Korea; mig2580@naver.com

* Correspondence: leechodg@scnu.ac.kr

Abstract: Titanium has many limitations in coverage and frequency of application due to its expensive alloying elements and complex manufacturing process. The biocompatible Ti-Mo-Fe ternary beta titanium alloys were designed by replacing high-cost beta-stabilizer elements (V, Nb, Zr, etc.) with low-cost Mo and Fe elements. In addition, it was attempted to obtain a low-cost, high-strength beta-titanium alloy with 800 MPa or more by applying the powder metallurgy process technology to the Ti-Mo-Fe alloy system. The added Mo element has the effect of reducing the elastic modulus of the titanium alloy without reducing its strength. In this study, Ti-Mo-Fe alloys designed with different Mo contents were fabricated using a powder metallurgy process and analyzed in connection with microstructural properties, phase changes, and mechanical properties. As Mo contents are increased, the α -lath thickness of Widmanstätten decreases and the size of prior β grain decreases. It was confirmed that the hardness and tensile strength were excellent and were compared with the ingot material of the same alloy system.



Citation: Hwang, H.-W.; Park, J.-H.; Lee, D.-G. Effect of Molybdenum Content on Microstructure and Mechanical Properties of Ti-Mo-Fe Alloys by Powder Metallurgy. *Appl. Sci.* **2022**, *12*, 7257. <https://doi.org/10.3390/app12147257>

Academic Editors: Junwon Seo and Jong Wan Hu

Received: 30 June 2022

Accepted: 15 July 2022

Published: 19 July 2022

Publisher's Note: MDPI stays neutral with regard to jurisdictional claims in published maps and institutional affiliations.



Copyright: © 2022 by the authors. Licensee MDPI, Basel, Switzerland. This article is an open access article distributed under the terms and conditions of the Creative Commons Attribution (CC BY) license (<https://creativecommons.org/licenses/by/4.0/>).

Keywords: Ti-Mo-Fe alloy; beta titanium; powder metallurgy; low cost; high strength

1. Introduction

Titanium has excellent specific strength and corrosion resistance and is widely used in aerospace, the defense industry, and biomaterials [1–5]. In particular, titanium has lower elastic modulus and higher specific strength than cobalt alloys, stainless steel, alumina, etc., and is widely used as biomaterials. However, commercially pure titanium (c.p. Ti) has comparatively low mechanical properties, such as tensile strength, making it unsuitable for certain applications. Further, it has been reported that the aluminum contained in a commercial titanium alloy, Ti-6Al-4V, can cause Alzheimer's disease [6], and vanadium can cause allergies and serious complications due to the release of toxic ions [7]. Therefore, it is required to develop biocompatible beta-titanium alloys in order to replace these components [8] and, at this time, niobium, zirconium, tantalum, and molybdenum are attracting attention as alloy elements that are not harmful to the human body [9]. Actually, many beta-titanium alloys, such as Ti-3Zr-5Fe-5Mo, Ti-14Mn, Ti-10Fe-10Ta, Ti-27Nb-7Fe-8Cr, Ti-33Zr-3Fe-4Cr, and Ti-7.5Mo, have been recently developed.

In fact, a beta-titanium alloy has excellent heat treatment characteristics compared to the $\alpha + \beta$ alloy and represents an increase in elongation due to its BCC structure, including a low elastic modulus, and then is used not only in biomaterials but also in various other fields. However, the β -stabilizer elements, tantalum, niobium, and zirconium, inevitably increase costs due to their expensive price, resulting in many restrictions on the use of beta titanium [10,11]. Thus, several studies have been actively conducted to replace expensive alloy elements, such as tantalum, niobium, and zirconium, with inexpensive elements (Fe, Mo, Mn, etc.) [12,13].

Iron, an inexpensive element, has a strong β -stabilizer effect and a good reinforcing effect on non-toxic and non-allergic titanium alloys [14]. In addition, it is reported to improve the sintering reaction of titanium alloys [15] because it represents a faster diffusion rate than the atom of titanium itself in the β phase as a rapidly diffused element [16]. Likewise, molybdenum is a biocompatible β -stabilizer element and when molybdenum is added to a titanium alloy, it has been reported to have high corrosion resistance [17–20], lower the elastic modulus, and increase the strength [21].

The titanium alloy obtained through the existing ingot metallurgy (IM) process results in significant process costs, such as multiple vacuum remelting, alloying additions, homogenization, hot deformation and annealing, etc. [22]. However, it is relatively easy to manufacture complex parts in a powder metallurgy (PM) process [23], and simpler work processes and facilities are used for comparing it with the ingot process. In addition, unlike the ingot process, Ti and alloy elements are heated to a temperature lower than the melting point, which has the advantage of significantly reducing costs [24,25].

Therefore, this study designed a biocompatible Ti-Mo-Fe high-strength beta-titanium alloy and applied the powder metallurgy process technology using hydrogenation–dehydrogenation (HDH) titanium powder to ensure excellent price competitiveness. Further, changes in the microstructure of the Ti-xMo-4Fe ($x = 3.4, 5$) powder alloys with different Mo contents were examined and then it was evaluated and analyzed in connection with mechanical properties. The results were compared with the properties of ingot alloys of the same alloy system.

2. Materials and Experiment

2.1. Alloy Design and Preparation

The Ti-xMo-4Fe ($x = 3.4, 5$) designed in this study is presented in the phase stability map ($\overline{Bo} - \overline{Md}$ map), Figure 1 [26]. The $\overline{Bo} - \overline{Md}$ map is a theoretical approach to the design of titanium alloys established by Morinaga et al. [27] and consists of two parameters. In addition, it can be clearly divided into α phase, $\alpha + \beta$, and β phase according to the alloy composition, and when the value of \overline{Bo} increases in the β phase and the value of \overline{Md} decreases, it becomes a stable state. The Bond order (\overline{Bo}) is a value representing the covalent bonding strength between the titanium and alloying elements and it is reported that as \overline{Bo} increases, the elastic modulus tends to decrease [28]. The Metal d-orbital energy level (\overline{Md}) is correlated with the electronegativity in the element. These two parameters can be calculated using the following Equation (1).

$$\overline{Md} = \sum_{i=1}^n X_i \cdot (Md)_i, \overline{Bo} = \sum_{i=1}^n X_i \cdot (Bo)_i \quad (1)$$

Using Equation (1), the values of the Metal d-orbital energy level (\overline{Md}) and Bond order (\overline{Bo}) of the Ti-3.4Mo-4Fe (hereinafter referred to as TMF 34) alloys were 2.39 and 2.79, respectively. Further, the values of the Ti-5Mo-4Fe (hereinafter referred to as TMF 54) alloys were 2.38 and 2.79, respectively.

The objective of this study is to compare the alloy designed in this study by applying the powder metallurgy (hereinafter referred to as P/M) and ingot metallurgy (hereinafter referred to as I/M) processes. In the case of the powder alloy, the HDH titanium powder was used to further reduce the cost of the titanium alloy. The powder used in P/M represented sizes of Ti (<25 μm), Mo (1–2 μm), and Fe (5–7 μm), which were blended and bound according to Ti-xMo-4Fe ($x = 3.4$, and 5 wt.%). It was blended using a mixer, pressed with a force of 200 kg/cm² for 15 s using a hydraulic press, and then the resulting bulk compacts were sintered in a sintering furnace for 5 h at 1250 °C. It was then furnace cooled to room temperature. Further, in order to compare it with ingots having the same alloy composition, ingots having a composition of Ti-xMo-4Fe ($x = 3.4, 5$) with a diameter of 14 mm were fabricated through applying a vacuum arc remelting method using Ti with

99.9% purity, Mo with 99.95% purity, and Fe with 99.5% purity. In the case of the porosity of the alloy applied to P/M, it was derived using Equation (2) [29].

$$P = \left[1 - \left(\frac{\rho}{\rho_0} \right) \right] \times 100 \quad (2)$$

where ρ and ρ_0 represent the apparent density and theoretical density in the P/M alloy measured using the Archimedeian method. The number of pores was measured using an optical microscope.

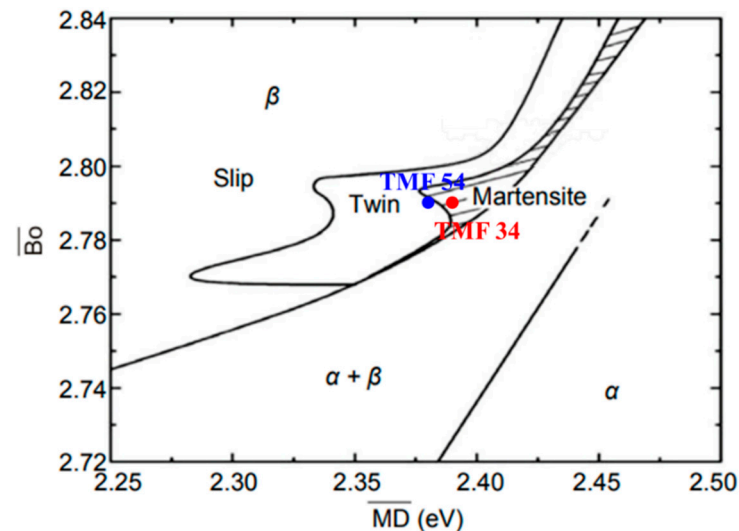


Figure 1. Bo and Md stability phase map showing the positions of the designed alloys [26].

2.2. Microstructural Characterization

In order to compare and analyze the microstructure of the designed alloys, Ti-xMo-4Fe ($x = 3.4, 5$ wt.%), the specimen was cut perpendicular to the longitudinal direction. The specimen was hot mounted for fine polishing and was finely polished using abrasive papers of #220~#2000, abrasives of 6 μm , 3 μm , and 1 μm , and colloid silica. Then, the specimen was etched by mixing 100 mL of distilled water (H_2O) with 2 mL of nitric acid (HNO_3) and 2 mL of hydrofluoric acid (HF). Using an optical microscope (OM, BX53M, Olympus, Tokyo, Japan) and an electron back-scattered diffraction pattern analyzer (EBSD, JSM-7100F, JEOL, Tokyo, Japan), the changes in microstructures according to the process method and Mo content were observed.

2.3. Mechanical Properties

The Vickers hardness test and room temperature tensile test were conducted to evaluate mechanical properties at room temperature. The hardness test was conducted using a Vickers hardness tester (HM-200, Mitutoyo, Kawasaki, Japan) and the average value excluding the maximum and minimum values was calculated by measuring 12 points while maintaining 1 kgf outward from the center of the designed alloy specimen for 15 s. The room temperature tensile test was conducted with a strain rate of $1 \times 10^{-3}/\text{s}$ by processing it with a tensile specimen standard of ASTM subsized using a room temperature tensile tester (Room Temperature Tensile Machine, BESTUTM-10MD, Ssaoul Bestech, Seoul, Korea).

3. Results and Discussion

3.1. Microstructural Characterization

The microstructures of the designed P/M alloys are presented in Figure 2a,b. Due to the furnace cooling after the sintering process, Widmanstätten, in which the dark α and light β phases were generated in a layered pattern in all P/M alloys and pores, were also

observed. In the case of the inside of TMF 34 I/M, $\alpha + \beta$ lamellar Widmanstätten structures were observed and the α phases precipitated within the equiaxed β grain inside of the TMF 54 I/M.

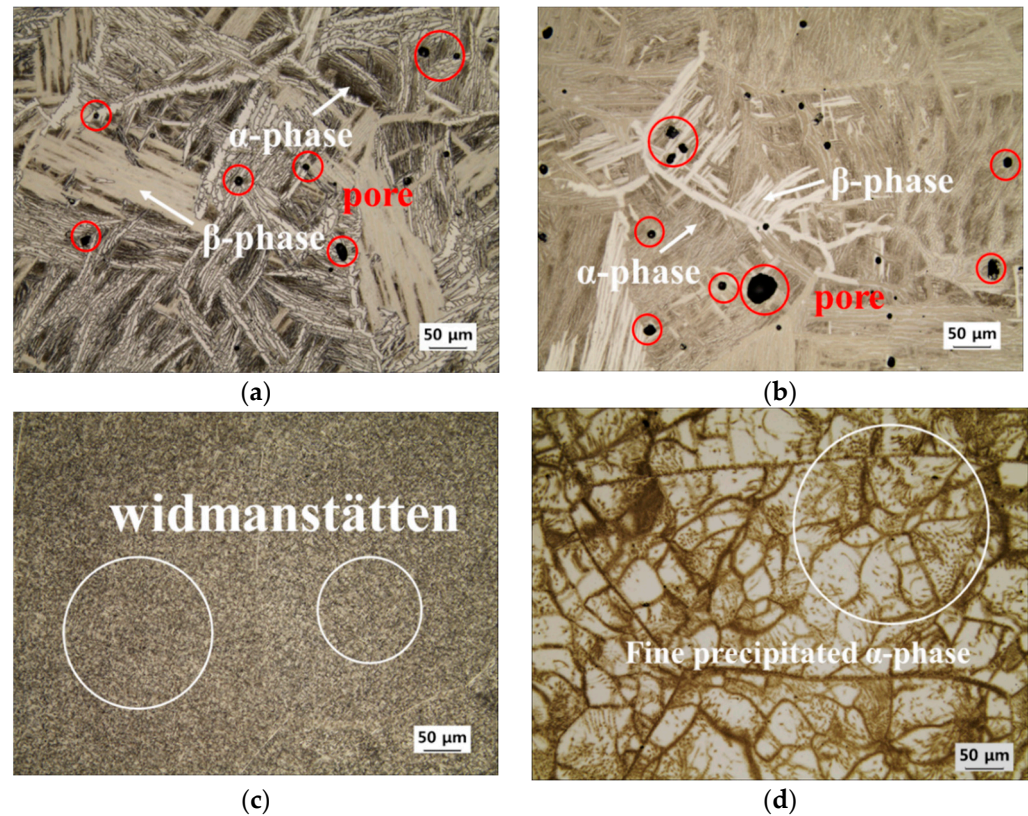


Figure 2. Optical micrographs of (a) TMF 34P/M, (b) TMF 54 P/M, (c) TMF 34 I/M, and (d) TMF 54 I/M.

In the case of the I/M alloy, the lamellar Widmanstätten microstructure with a $\alpha + \beta$ was observed in TMF 34 I/M, and in the case of TMF 54 I/M, the α -phase precipitated inside equiaxed β grain had different structures (Figure 2c,d). In the case of the Widmanstätten structure, cracks are first generated at the boundary of colony or grain boundary α -phase and it is reported that cracks are propagated in this way and its tensile ductility is low [30]. In the equiaxed structure, cracks occur mainly at the interface of α/β , resulting in high strain. Therefore, it is expected that TMF 54 I/M with the equiaxed structure represents higher strain than TMF 34 I/M with the $\alpha + \beta$ lamellar Widmanstätten.

Figure 3 shows an observation of the Inverse pole figure (IPF) map for analyzing the Widmanstätten observed in the P/M alloys. The thickness of the Widmanstätten α -lath of TMF 34 P/M was measured to be 12.289 μm and the thickness of the Widmanstätten α -lath of TMF 54 P/M was measured to be 10.547 μm . It can be seen that as the Mo content increases, the thickness of the Widmanstätten α -lath becomes thinner. Mo is one of the β -stabilizer elements and the temperature in the β transformation point decreases. In this study, when furnace cooling is performed after the sintering process at 1250 $^{\circ}\text{C}$, the exposure time to the β transformation temperature increases according to the increase in the Mo content. Therefore, the fraction rate of the β phase increases, and accordingly, it is determined that the thickness of the Widmanstätten α -lath decreased as the time of exposure to the α phase decreased. In the practical observation of the EBSD phase map of the TMF 34 and TMF54 alloys, it was confirmed that the fraction rate of the α phase decreased from 56% to 50.4% and the fraction of the β phase increased from 44% to 49.6% (Figure 4).

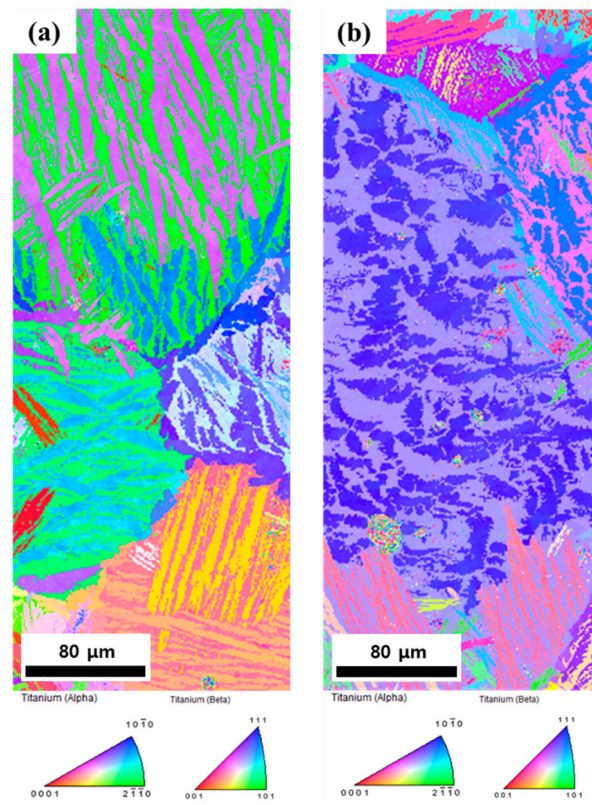


Figure 3. Inverse pole figure (IPF) maps of (a) TMF 34 P/M and (b) TMF 54 P/M.

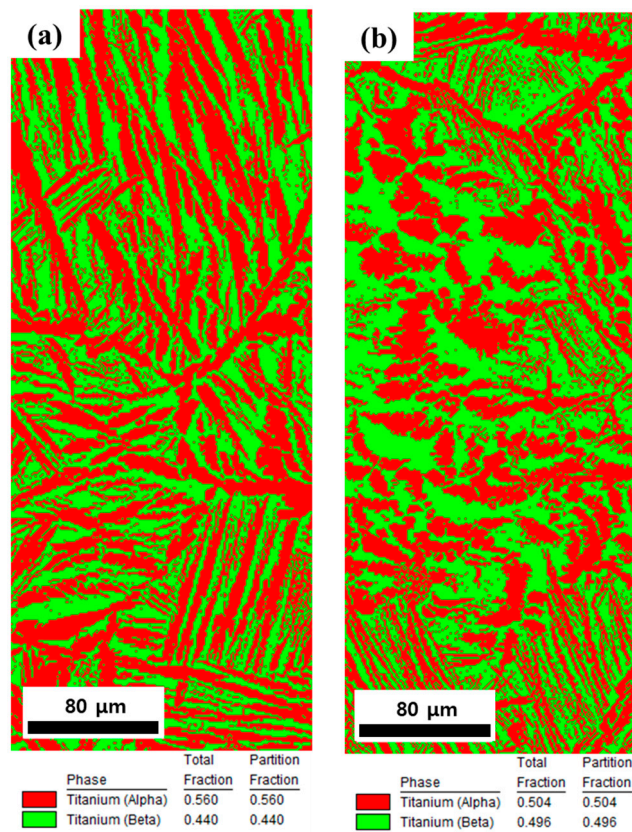


Figure 4. EBSD analysis of phase map of (a) TMF 34 P/M and (b) TMF 54 P/M.

Figure 5 shows the pore analysis table observed in the P/M alloys. Small pores below 10 μm are mainly due to the ‘Kirkendal’ effect in powder metallurgy and are caused by atomic mutual diffusion during a solid-phase sintering process [31]. While pores with sizes of 40 μm or more were not observed in TMF 34 P/M, pores with sizes of 40 μm to 45 μm were observed in TMF 54 P/M. As a result of analyzing the pore distribution, the pore fraction rate increased by about 1.4% from 2.1% to 3.5% as the content of Mo increased. This is due to the low-diffusion coefficient of Mo and the diffusion rate of Mo in Ti particles is slower than that of Ti itself. Therefore, the addition of Mo interferes with the sintering reaction and is sensitive to the formation of Kirkendall pores [31,32]. Thus, the pore fraction rate of the TMF 54P/M alloy was measured to be 1.4% higher because the Mo content of TMF 54P/M was increased more than that of TMF 34P/M. In addition, it is known that the low diffusivity of Mo interferes with the movement of the particle boundary and affects grain refinement [33].

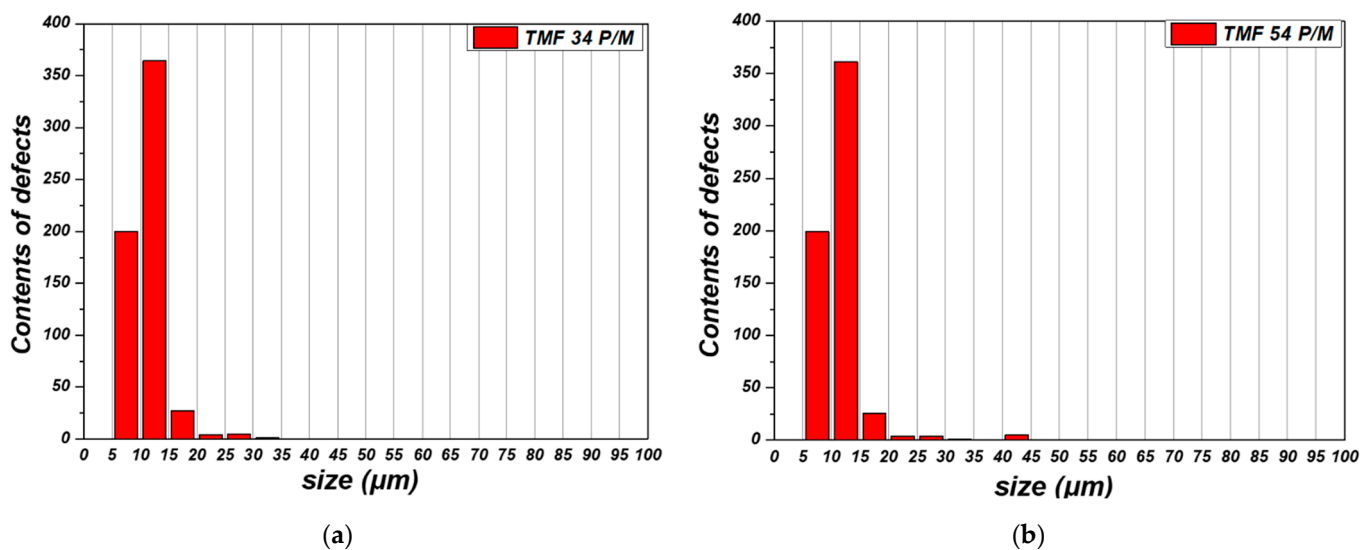


Figure 5. Distribution of pore size and pore amount in (a) TMF 34 P/M and (b) TMF 54 P/M alloys.

According to the IPF map in Figure 6, schematized by measuring the misorientation of the TMF design alloy, the size of the prior β grain decreased from 226.55 μm to 211.99 μm when the Mo content increased from the actual TMF 34 P/M to TMF 54 P/M. The prior β grain size is an important factor that can significantly affect mechanical properties. Because it relies significantly on the prior β grain size, the grain control is essential. In fact, it is known that the maximum tensile strength and yield strength increase according to the decrease in the prior β grain size [34].

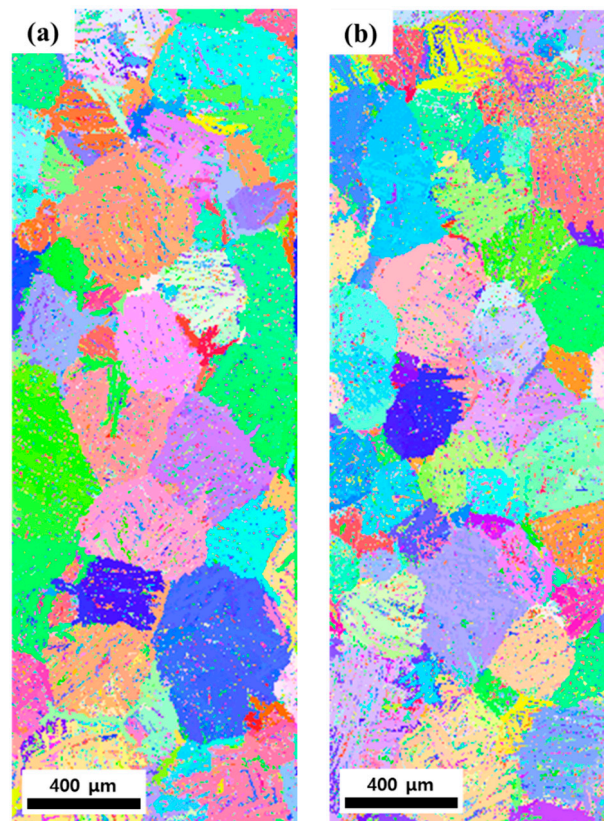


Figure 6. IPF maps of prior β grains reconstructed by misorientation criterion and denoising method (a) TMF 34 P/M and (b) TMF 54 P/M.

3.2. Mechanical Properties

Figure 7 shows the results of measuring Vickers hardness for four types of TMF β alloys manufactured according to the alloy composition and process method. In the case of the P/M alloy, it was determined that the hardness values of TMF 34 P/M and TMF 54 P/M were 397.5 Hv and 396.5 Hv, respectively, which slightly decreased when the Mo content increased. In general, it is known that as the Mo content increases, the hardness value increases due to the solid-solution strengthening effect [35], but when the Mo content increases, the hardness value increases due to the decrease in the thickness of Widmanstätten α -lath and the pore fraction increases (2.1% \rightarrow 3.5%). As a result, the effect of decreasing the hardness value was largely affected and it is considered that the hardness value of TMF 54 P/M was similar to the hardness value of TMF 34 P/M.

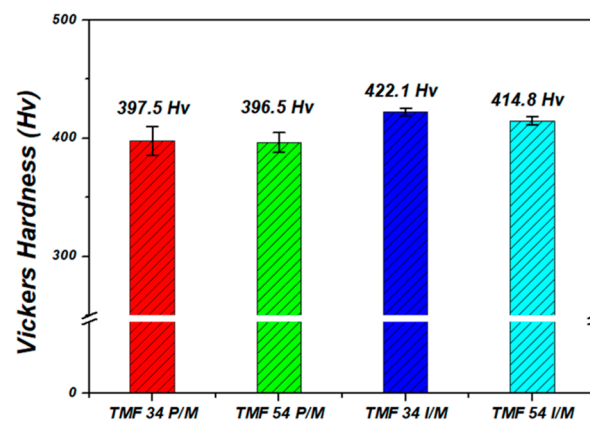


Figure 7. Vickers hardness of TMF 34 and TMF 54 alloys.

In addition, in the case of the I/M alloy, the hardness values of TMF 34 I/M and TMF 54 I/M are 422.1 Hv and 414.8 Hv, respectively, where the hardness value of TMF 34 I/M is slightly higher than that of TMF 54 I/M. In the case of TMF 34 I/M, it is an $\alpha + \beta$ lamellar Widmanstätten microstructure. In the case of TMF 54 I/M, it is a relatively soft α -phase precipitated in the equiaxed β grain. Therefore, in the case of the I/M alloy, the hardness value of TMF 34 I/M was measured higher than the hardness value of TMF 54 I/M. In addition, the P/M alloy has a hardness value lower than that of I/M with the same composition and the hardness of the P/M alloy is decreased due to pores in the P/M alloy. Thus, it is considered that the hardness value of the P/M alloy is lower than that of the ingot alloy.

The tensile stress–strain curves obtained from the room temperature tensile test conducted on four types of the TMF beta alloys are shown in Figure 8 and the tensile characteristic values (yield strength, ultimate tensile strength, and elongation) measured from the curve are shown in Table 1. All P/M alloys were fractured before the yield point, and mechanical strength and elongation were measured lower than those of the I/M alloys. This shows that the fracture occurred before the yield point due to pores and the fracture surface shows a cleavage fracture form in all P/M alloys. It can be seen that cracks started from these pores (Figure 9a,b). In addition, the ultimate tensile strength of TMF 54 P/M was 815.27 MPa, which was higher than that of TMF 34 P/M. The cause is considered to be the influence of the prior β grain size and the strength increases according to the Hall–Petch equation because the prior β grain size is small [36].

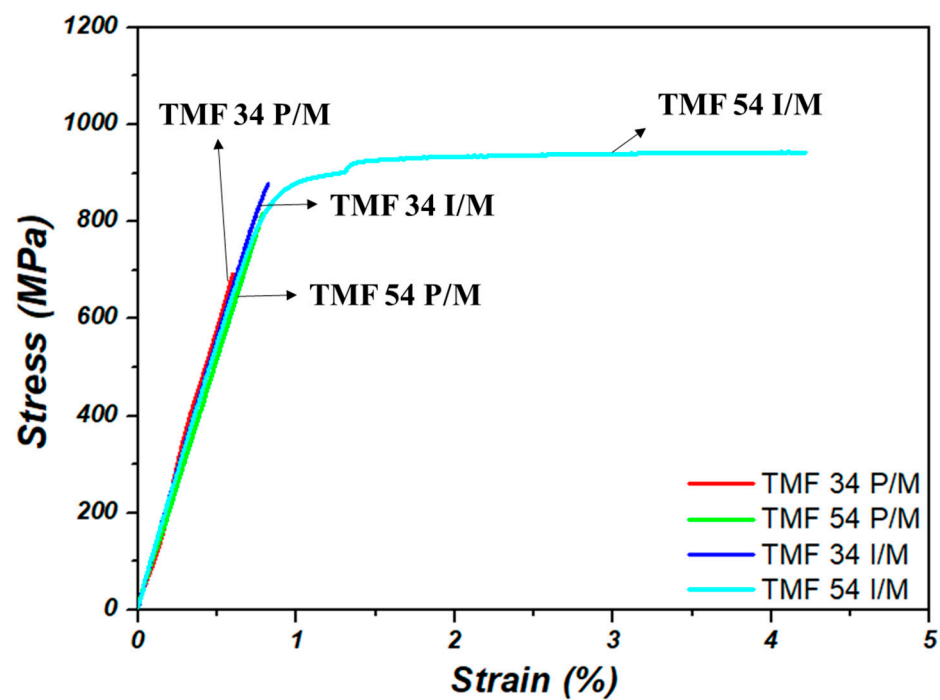


Figure 8. Tensile stress–strain curve of TMF 34 and TMF 54 alloys.

Table 1. Tensile properties of TMF 34 and TMF 54 alloys.

	Yield Strength (MPa)	Ultimate Strength (MPa)	Elongation (%)
TMF 34 P/M	-	692.69	0.60
TMF 54 P/M	-	815.27	0.79
TMF 34 I/M	-	877.15	0.82
TMF 54 I/M	821.29	942.51	4.20

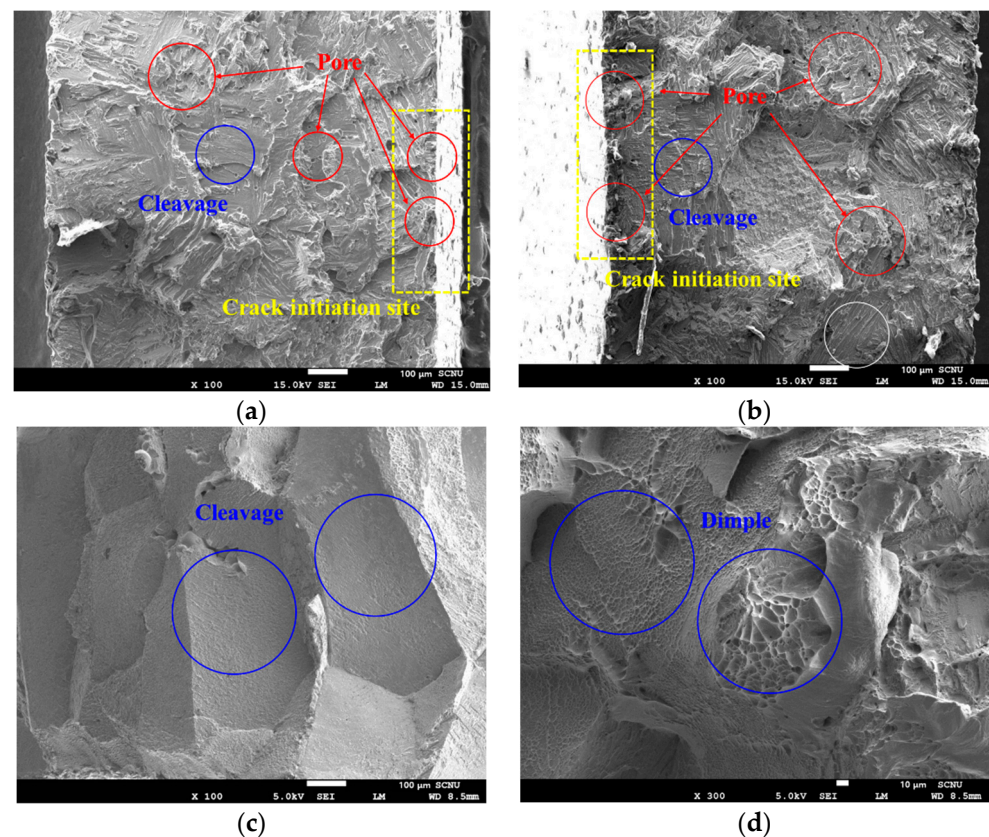


Figure 9. SEM images of the fractured surface of (a) TMF 34 P/M, (b) TMF 54 P/M, (c) TMF 34 I/M, and (d) TMF 54 I/M.

In the case of the I/M alloy, TMF 54 I/M has the equiaxed β grain with a relatively soft microstructure. As mentioned above, in the equiaxed microstructure, it is reported that the slips are strengthened due to the interference in the movement caused by the α phases precipitating inside the equiaxed β grain, and not only slips but also twins act as a deformation mechanism, contributing to the increase in elongation [34]. Therefore, the TMF 54 I/M alloys with the equiaxed microstructure represents higher elongation than the TMF 34 I/M alloys with $\alpha + \beta$ lamellar Widmanstätten microstructure. As shown in Figure 9c,d, some dimple structures, which indicate a ductile fracture behavior, were observed on the fracture surface of TMF 54 I/M. However, in the case of TMF 34 I/M, the cleavage fracture surface, a characteristic of brittle fracture behavior, was observed.

4. Conclusions

In this study, ternary beta-titanium alloys with a tensile strength of 800 MPa or higher were designed by replacing alloy elements, Al and V, with biocompatible Mo and Fe. Ti-Mo-Fe alloys were fabricated by applying a powder metallurgy process, and microstructure and mechanical properties according to Mo content were considered. The major results are summarized as follows.

1. It is possible to secure excellent price competitiveness by successfully developing Ti-Mo-Fe P/M alloys by adding low-cost Mo and Fe, which can fabricate complex parts and reduce costs. The cost of alloying elements is reduced by 81–84% and 63–67% compared to the widely used Ti-6Al-4V and Ti-13Nb-13Zr alloys, respectively. Further, the cost may be further reduced by using HDH powder.
2. In the case of TMF 34 I/M, an $\alpha + \beta$ lamellar Widmanstätten microstructure was observed, and in the case of TMF 54 I/M, an α phase precipitating inside the equiaxed β grain was observed. In the equiaxed microstructure, where cracks occur mainly at the α/β interface, deformation can be generated by slips and twins. Further, it is

reinforced by the precipitated fine α phase according to an increase in Mo content, showing high tensile strength and elongation in the TMF 54 I/M alloys.

3. According to the increase in Mo content, TMF 34 P/M \rightarrow TMF 54 P/M, the thickness of the Widmanstätten α -lath decreases (12.289 μm \rightarrow 10.547 μm) and the size of prior β grains decrease (226.55 μm \rightarrow 211.99 μm). For this reason, it was possible to obtain excellent tensile strength of 800 MPa or more, even though the pore fraction increased (2.1% \rightarrow 3.5%) as the Mo content increased.
4. Tensile fractures occurred in the elastic region before the yield point due to pores in both the TMF 34 P/M and TMF 54 P/M alloys, and the change in Mo content was analyzed with I/M alloys by the E and σ reinforcing mechanisms.

Author Contributions: Conceptualization, H.-W.H. and D.-G.L.; methodology, H.-W.H. and D.-G.L.; validation, H.-W.H., J.-H.P. and D.-G.L.; formal analysis, H.-W.H., J.-H.P. and D.-G.L.; investigation, H.-W.H. and D.-G.L.; writing—original draft preparation, H.-W.H.; writing—review and editing, D.-G.L.; supervision, D.-G.L.; funding acquisition, J.-H.P. and D.-G.L. All authors have read and agreed to the published version of the manuscript.

Funding: This research received no external funding.

Institutional Review Board Statement: Not applicable.

Informed Consent Statement: Not applicable.

Data Availability Statement: All data are available within the manuscript.

Acknowledgments: This work was supported by the Korean government MOTIE (the Ministry of Trade, Industry and Energy), the Korea Evaluation Institute of Industrial Technology (KEIT) (No. 20010047), and the Korea Institute for Advancement of Technology (KIAT) (No. P0002019).

Conflicts of Interest: The authors declare no conflict of interest.

References

1. Leyens, C.; Peters, M. *Titanium and Titanium Alloys: Fundamentals and Applications*, 1st ed.; betz-druck GmbH: Darmstadt, Germany, 2004.
2. Rehman, A.U.; Kishore Babu, N.; Talari, M.K.; Usmani, Y.; Alkhalefah, H. Characterisation of Microstructure and Mechanical Properties of Linear Friction Welded $\alpha+\beta$ Titanium Alloy to Nitinol. *Appl. Sci.* **2021**, *11*, 10680. [[CrossRef](#)]
3. Lütjering, G.; Williams, J.C. *Titanium*, 2nd ed.; Springer: Berlin/Heidelberg, Germany; New York, NY, USA, 2007; pp. 383–415.
4. Hwang, Y.-J.; Park, Y.-K.; Kim, C.-L.; Kim, J.-Y.; Lee, D.-G. Mechanical Properties Variation of Ti-6Al-4V Alloys by Microstructural Control. *J. Korean Soc. Heat Treat.* **2016**, *29*, 220–226. [[CrossRef](#)]
5. Yang, S.; Su, S.; Liu, X.; Han, P. Study on Milling Temperature of Titanium Alloy with Micro-Textured Ball End Milling Cutter under Radius of Blunt Edge. *Appl. Sci.* **2020**, *10*, 587. [[CrossRef](#)]
6. Walker, P.R.; LeBlanc, J.; Sikorska, M. Effects of aluminum and other cations on the structure of brain and liver chromatin. *Biochemistry* **1989**, *28*, 3911–3915. [[CrossRef](#)]
7. Manam, N.; Harun, W.; Shri, D.; Ghani, S.; Kurniawan, T.; Ismail, M.H.; Ibrahim, M. Study of corrosion in biocompatible metals for implants: A review. *J. Alloys Compd.* **2017**, *701*, 698–715. [[CrossRef](#)]
8. Hwang, Y.J.; Lee, D.G. Effect of Al Addition on Corrosion Protection of Ti-39Nb-6Zr Alloy for Biological Applications. *J. Nanosci. Nanotechnol.* **2019**, *19*, 3811–3815. [[CrossRef](#)] [[PubMed](#)]
9. Li, Y.; Yang, C.; Zhao, H.; Qu, S.; Li, X.; Li, Y. New developments of Ti-based alloys for biomedical applications. *Materials* **2014**, *7*, 1709–1800. [[CrossRef](#)]
10. Allen, P.G.; Bania, P.J.; Hutt, A.J.; Combres, Y. Titanium '95 Science and Technology. In Proceedings of the Eighth World Conference on Titanium, International Convention Centre, Birmingham, UK, 22–26 October 1995; Blenkinsop, P.A., Evans, W.J., Flower, H.M., Eds.; The Institute of Metals: London, UK, 1996.
11. Lee, Y.T. *Titanium*; Steel & Metal News Co., Ltd.: Seoul, Korea, 2009; pp. 61–128.
12. Gepreel, M.; Niinomi, M. Biocompatibility of Ti-alloys for long-term implantation. *J. Mech. Behav. Biomed. Mater.* **2013**, *20*, 407–415. [[CrossRef](#)]
13. Ehtemam-Haghighi, S.; Attar, H.; Okulov, I.V.; Dargusch, M.S.; Kent, D. Microstructural evolution and mechanical properties of bulk and porous low-cost Ti–Mo–Fe alloys produced by powder metallurgy. *J. Alloys Compd.* **2021**, *853*, 156768. [[CrossRef](#)]
14. Bao, Y.; Zhang, M.; Liu, Y.; Yao, J.; Xiu, Z.; Xie, M.; Sun, X. High strength, low modulus and biocompatible porous Ti–Mo–Fe alloys. *J. Porous Mater.* **2014**, *21*, 913–919. [[CrossRef](#)]
15. Nakajima, H.; Koiwa, M. Diffusion in titanium. *ISIJ Int.* **1991**, *31*, 757–766. [[CrossRef](#)]

16. Jindal, V.; Sarda, A.; Degnah, A.; Chandran, K.R. Effect of iron & boron content on the Spark Plasma Sintering of Ti-B-Fe alloys. *Adv. Powder Technol.* **2019**, *30*, 423–427.
17. Ho, W.-F. A comparison of tensile properties and corrosion behavior of cast Ti–7.5Mo with c.p. Ti, Ti–15Mo and Ti–6Al–4V alloys. *J. Alloys Compd.* **2008**, *464*, 580–583. [[CrossRef](#)]
18. Sugano, M.; Tsuchida, Y.; Satake, T.; Ikeda, M. A microstructural study of fatigue fracture in titanium–molybdenum alloys. *Mater. Sci. Eng. A* **1998**, *243*, 163–168. [[CrossRef](#)]
19. Kumar, S.; Tsn, S.N. Electrochemical characterization of β -Ti alloys in Ringer’s solution for implant application. *J. Alloys Compd.* **2009**, *479*, 699–703. [[CrossRef](#)]
20. Lin, D.-J.; Chuang, C.-C.; Chern Lin, J.-H.; Lee, J.-W.; Ju, C.-P.; Yin, H.-S. Bone formation at the surface of low modulus Ti–7.5Mo implants in rabbit femur. *Biomaterials* **2007**, *28*, 2582–2589. [[CrossRef](#)]
21. Santos, P.F.; Niinomi, M.; Liu, H.; Cho, K.; Nakai, M.; Trenggono, A.; Champagne, S.; Hermawan, H.; Narushima, T. Improvement of microstructure, mechanical and corrosion properties of biomedical Ti-Mn alloys by Mo addition. *Mater. Des.* **2016**, *110*, 414–424. [[CrossRef](#)]
22. Carman, A.; Zhang, L.; Ivasishin, O.; Savvakina, D.; Matviychuk, M.; Pereloma, E. Role of alloying elements in microstructure evolution and alloying elements behaviour during sintering of a near-beta titanium alloy. *Mater. Sci. Eng. A* **2011**, *528*, 1686–1693. [[CrossRef](#)]
23. Menhal Shbeh, M.; Yerokhin, A.; Goodall, R. Microporous Titanium through Metal Injection Moulding of Coarse Powder and Surface Modification by Plasma Oxidation. *Appl. Sci.* **2017**, *7*, 105. [[CrossRef](#)]
24. Santos, D.; Pereira, M.d.S.; Cairo, C.; Graca, M.; Henriques, V. Isochronal Sintering of the Blended Elemental Ti-35Nb Alloy. *Mater. Sci. Eng. A* **2008**, *472*, 193–197. [[CrossRef](#)]
25. Bolzoni, L. Low-cost Fe-bearing powder metallurgy Ti alloys. *Met. Powder Rep.* **2019**, *74*, 308–313. [[CrossRef](#)]
26. Kuroda, D.; Niinomi, M.; Morinaga, M.; Kato, Y.; Yashiro, T. Design and mechanical properties of new β type titanium alloys for implant materials. *Mater. Sci. Eng. A* **1998**, *243*, 244–249. [[CrossRef](#)]
27. Morinaga, M.; Kato, M.; Kamimura, T.; Fukumoto, M.; Harada, I.; Kubo, K. Theoretical design of beta-type titanium alloys. In *Titanium’92: Science and Technology*; The Minerals, Metals & Materials Society: Pittsburgh, PA, USA, 1993; pp. 217–224.
28. Abdel-Hady, M.; Hinoshita, K.; Morinaga, M. General approach to phase stability and elastic properties of β -type Ti-alloys using electronic parameters. *Scr. Mater.* **2006**, *55*, 477–480. [[CrossRef](#)]
29. Xu, J.; Bao, L.; Liu, A.; Jin, X.; Tong, Y.; Luo, J.; Zhong, Z.; Zheng, Y. Microstructure, mechanical properties and super elasticity of biomedical porous Ni Ti alloy prepared by microwave sintering. *Mater. Sci. Eng. C* **2015**, *46*, 387–393. [[CrossRef](#)]
30. Bae, K.-M.; Park, C.-G.; Chang, Y.-W.; Lee, C.-S. The Effect of α -Phase Morphology on the Microcrack Initiation Behavior of a Ti-6Al-4V Alloy. *Korean J. Met. Mater.* **1993**, *31*, 105–112.
31. Tang, C.Y.; Zhang, L.N.; Wong, C.T.; Chan, K.C.; Yue, T.M. Fabrication and characteristics of porous NiTi shape memory alloy synthesized by microwave sintering. *Mater. Sci. Eng. A* **2011**, *528*, 6006–6011. [[CrossRef](#)]
32. Liu, Y.; Chen, L.; Tang, H.; Liu, C.T.; Liu, B.; Huang, B. Design of powder metallurgy titanium alloys and composites. *Mater. Sci. Eng. A* **2006**, *418*, 25–35. [[CrossRef](#)]
33. Zhang, W.; Xie, H.; Hui, S.; Ye, W.; Yu, Y.; Song, X.; Peng, L.; Huang, G.; Yang, Z. In-Situ SEM Observation on Fracture Behavior of Titanium Alloys with Different Slow-Diffusing β Stabilizing Elements. *Materials* **2020**, *13*, 1848. [[CrossRef](#)]
34. Tiley, J.; Searles, T.; Lee, E.; Kar, S.; Banerjee, R.; Russ, J.C.; Fraser, H.L. Quantification of microstructural features in α/β titanium alloys. *Mater. Sci. Eng. A* **2004**, *372*, 191–198. [[CrossRef](#)]
35. Lee, E.B.; Han, M.K.; Kim, B.J.; Song, H.J.; Park, Y.J. Effect of molybdenum on the microstructure, mechanical properties and corrosion behavior of Ti alloys. *Int. J. Mater. Res.* **2014**, *105*, 847–853. [[CrossRef](#)]
36. Chong, Y.; Bhattacharjee, T.; Shibata, A.; Tsuji, N. Investigation of the grain size effect on mechanical properties of Ti-6Al-4V alloy with equiaxed and bimodal microstructures. *IOP Conf. Ser. Mater. Sci. Eng.* **2017**, *219*, 012013. [[CrossRef](#)]